In Situ Generation of Fullerene from a Poly(fullerene)

Hugo Santos Silva, Hasina Ramanitra, Bruna Bregadiolli, Aurélien
Tournebize, Didier Bégué, Simon Dowland, Christine Lartigau-Dagron, Carlos
Graeff, Andreas Distler, Heiko Peisert, et al.

In-situ generation of fullerene from a poly(fullerene)

Hugo Santos Silva,[1,2] Hasina H. Ramanitra,[1,2] Bruna A. Bregadiolli,[1,3] Aurélien Tournebize,[2] Didier Bégué,[1] Simon A. Dowland,[4] Christine Lartigau-Dagron,[1] Carlos F. O. Graeff,[3] Andreas Distler,[4] Heiko Peisert,[2] Thomas Chassé,[2] Roger C. Hiorns[1*]

[1]   CNRS/Univ Pau & Pays Adour, Institut des Science Analytiques et Physico-Chimie pour l'Environnement et les Materiaux, Pau, France.
[2]   Institute for Physical and Theoretical Chemistry, Eberhard Karls Universität Tübingen, Auf der Morgenstelle 18, 72076 Tübingen, Germany.
[3]   Departamento de Física – FC – UNESP, Av. Luiz Edmundo Carrijo Coube, 14-01, 17033-360 Bauru, Brazil.
[4]   BELECTRIC OPV GmbH (now OPVIUS GmbH), Landgrabenstraße 94, 90443 Nürnberg, Germany.
Present address: Bavarian Center for Applied Energy Research, Solar Factory of the Future, Fürther Str. 250, 90429 Nürnberg, Germany.

*roger.hiorns@univ-pau.fr

Abstract

This paper appraises the thermal, photo- and photo-oxidative stability of poly(fullerene)-*alt*-[bismethylbenzene)]s (PFBMBs) prepared by the atom transfer radical addition polymerisation (ATRAP) with particular attention paid to their use as additives in organic photovoltaic devices. PFBMBs are of interest due to their well-defined structures based on alternating, main-chain, fullerene-methylene links. This work shows by way of a wide range of characterisation techniques and a small library of PFBMBs with varying side-chains, however, that PFBMBs are relatively unstable. Given that prior work has shown that other main-chain fullerene polymers, such as poly(pyrrolidinofullerene)s, are inherently stable, we suggest a degradation mechanism specific to the fullerene-methylene links of PFBMBs which explains their unusual behaviour. This work suggests that polymers based on fullerene each have their own specific stabilities and qualities and that PFBMBs might be of more use in purposes other than OPVs where *in-situ* delivery of fullerene is required, for example, in medical applications.

Keywords: poly(fullerene); organic solar cell; organic photovoltaic; atom transfer radical addition polymerisation (ATRAP)

TOC
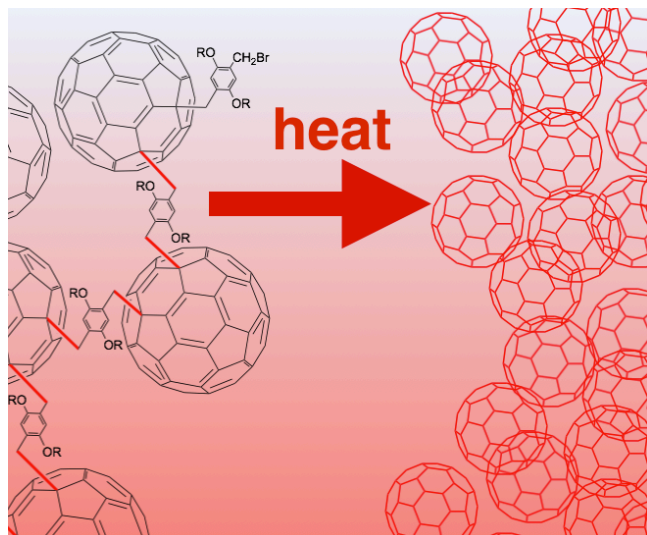
TOC short text
Fullerenes linked in a chain by single methylene bonds are found to be thermally unstable due to the low C_{60}-CH_2 bond energy. This property might be of use for *in-situ* delivery of fullerene, such as in medical applications, and is in stark contrast to other main-chain poly(fullerene)s which for the most part are extremely stable.

1   Introduction

The mechanisms involved in the photovoltaic effect in organic layers require both an optimised crystallization of electron donor and acceptor materials and their good miscibility to form a third mixed phase.[1] This promotes the dissociation of charges, formed from excitonic states, and their subsequent transfer to the electrodes.[2] Device lifetimes and efficiencies are often problematic because of the tendency of the two materials in the active-layer to phase-separate rather than form an ideal bi-continuous inter-penetrating network.[3] In effect, the donor and acceptor materials are in an unstable composite.[4] To some extent, this "like-likes-like" behaviour can be controlled by annealing treatments[5] and processing additives,[6] however, the mixture will always remain sensitive to environmental changes, and strategies to compatibilise and stabilise the donor and acceptor demixing remain highly desirable.

The stability of organic photovoltaic (OPV) devices can now be resolved by using encapsulation to slow the penetration of water and oxygen,[7,8] such that commercial cells can attain 15 year lifetimes.[9] The sensitivity of the active components to photo-oxidation can also be reduced by decreasing the lability of macromolecular hydrogens which are the most readily attacked sites.[10] Similarly, the careful pairing of acceptors and donors can influence susceptibilities to degradation.[11] However, it is difficult to control the heat that can impact on the morphologically of the active-layer during device operation.

Studies on the thermal degradation of bulk-heterojunction OPVs have mainly dealt with the donor-acceptor pair of poly(3-hexylthiophene) and [6,6]-phenylC$_{61}$ butyric acid methyl ester (P3HT:PCBM),[12] but also with low-band gap donor polymers (LBGs) combined with either PCBM[13] or non-fullerene acceptors (NFAs).[14] It remains important to improve the understanding of fullerenes' behaviours given that the very highest efficiencies have been attained using both NFAs and fullerenes.[15] A key problem with PCBM is that the fullerene derivatives leach from and migrate through the donor matrix to aggregate in clusters and crystals to reduce device efficiency.[16-18] Several techniques to arrest this process have come about, such as by varying the donor polymer side-chains,[19] or using additives, which limit the scale of the clusters through nucleation.[20] While additives are of great use with the crystalline donor polymers, more amorphous LBG polymers pose several problems in terms of restraining the movement of the C$_{60}$-based acceptors during a so-called burn-in. This process, mostly associated with fullerene-dimerisation, results in a drop in device efficiency in the first few hours of operation.[21] For PCBM-based OPVs at least, the use of poly(fullerene)s (PFs) has reduced the impact of burn-in for both amorphous LBG polymers and the more crystalline LBG and P3HT counterparts.[22] PF-based block copolymers have shown even greater promise in improving stabilities when used as additives.[23,24]

PFs contain C_{60} in the main-chain and are formed by pre-modification of C_{60} and subsequent polycondensation with functionalised comonomers,[25] or by direct reaction of comonomers with C_{60}.[26] The latter is preferred due to its simplicity. To our knowledge six methodologies have been found that can make main-chain PFs by direct reactions. All lead to alternating copolymers based on $(C_{60}$-comonomer$)_n$ repeating units and each results in oligomers and polymers with particular properties arising from the type of comonomer used and the way in which the C_{60} is modified by the addition. The first PF was made by thermally-assisted coupling of C_{60} and xylyene and was mostly an insoluble, crosslinked material.[27] The first easily accessible main-chain copolymer was made with Diels-Alder chemistry between bis-1,2-quinodimethanes and C_{60} and had up to around 80 C_{60}s, however, quite large degrees of crosslinking were found.[28] So-called amino-fishing, controlled by the use of large cyclodextrins innovatively formed the first water-soluble chains.[29] More recently, the first main-chain polymers based on C_{60} derivatives such as PCBM,[30] or at lower molecular weights, C_{60} and dyes,[31] were made using so-called Prato chemistry in the sterically controlled azomethine ylide cycloaddition polymerisation (SACAP). However, the polymers formed by this route are regio-irregular polymers due to a variety of positional attacks on the C_{60} sphere. In another route, oligomers with well-defined additions to the C_{60}, but as yet variable solubilities can be formed using azide chemistry.[32] Finally, while typically yielding oligomers, the atom transfer radical addition polymerisation (ATRAP) of C_{60} is of interest as it delivers PFs in reasonable yields with well-controlled structures.[33] The ATRAP reaction itself has been described in-depth elsewhere, and will not be detailed here, suffice to say that comonomers add in pairs around a single C_{60} phenylene ring by way of a controlled radical addition mechanism. Steric exclusion created by the first pair of additions, coupled with a favourable ratio of reagents, tends to limit the attack of more comonomers to the C_{60}, making it possible to form linear oligomers and polymers. Further details are given in reference 34.

Recent work employing the ATRAP route gave rise to main-chain PCBM-based oligomers, and these materials were shown to well-stabilise both crystalline and amorphous low band gap polymers for OPVs. We also calculated that analogous ATRAP-PFs based on C_{60} i.e., with the structure poly{(fullerene)-*alt*-[1,4-bis(methyl)-2,5-di(alkyloxy)benzene]} (PFBMB) would have electronic properties similar to those of PCBM. Therefore, we prepared a small library of PFBMBs to understand how variations in side-chains influence the formation of oligomers and polymers.[34] We were interested to see if these new C_{60} based PFBMBs would also stabilise devices. Furthermore, the stability of this recently discovered class of materials is poorly understood; indeed, to our knowledge, no study has looked at how variations in side-chains contribute to any class of PFs' physico-chemical properties. Thus, this work takes the same small library of PFBMBs formed by the ATRAP route, tries to correlate their structures against the resulting variations in physical and organic photovoltaic

properties, and by studying one sample in detail tries to understand the particularities of PFs made using the ATRAP route.

2 Results and Discussion

2.1 Materials

It was decided to study a small library of structures with varying side-chains to see if these impacted on the polymer stabilities. Cyclic, branched and different linear alkyl groups were used so that the impact of these variations could be compared. The use of a simple comonomer, 1,4-dialkoxy-2,5-dimethylene-phenylene, also meant these lateral chains could be easily changed to yield the library of PFBMBs shown in Table 1. The methylene links between the fullerene and the phenylene of the comonomer differentiates these materials from other classes of PFs, which are often based on robust cyclic bonds. The samples that were used in this study are the same as those characterised (GPC, NMR, UV-visible, cyclic voltammetry etc.) in detail in reference 34, and accordingly the same code for each structure is used.
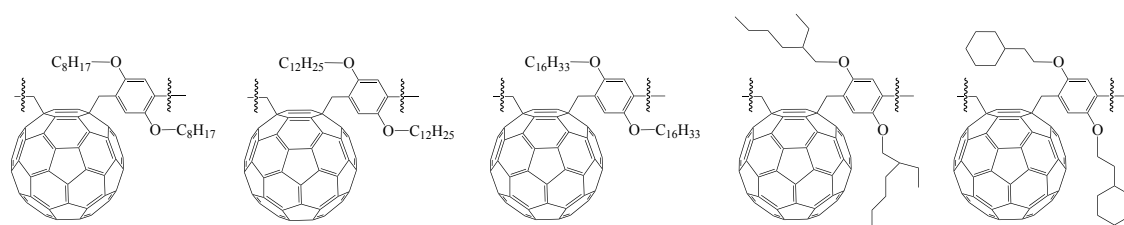
label	HSS-8	HSS-12	HSS-16	HSS-B8	HSS-C8
M_p (g mol^{-1})[a]	b	16700	21000	13000	b
E_{LUMO} (eV)[b]	-3.38	-3.38	-3.41	-3.39	-3.39

Table 1. Structures of the repeating units of the oligomeric and polymeric PFBMBs studied in this work. The details given are summaries from reference 34. Notes: (a) as indicated by GPC and self-consistent calibration against oligomers (THF, RI, 30 ˚C); (b) lower solubilities limited characterisation of M_p, however, NMRs indicated weights comparable to HSS-8; (c) cyclic voltammetry from solutions in 1,2-dichlorobenzene/acetonitrile (4:1 v/v) with tetrabutylammonium hexafluorophosphate (0.1 M). Under the same conditions, PCBM was found to have E_{LUMO} = -3.8 eV.

2.2 Impact of PFBMBs on Photovoltaic Device Efficiencies and Stabilities

The polymers were employed with poly(3-hexylthiophene) (P3HT) in inverted OPV devices with the general architecture ITO/ZnO/P3HT:PCBM/PEDOT:PSS/Ag. Complete details of the device assembly are given in the Supporting Information (SI). The PFBMBs are used here in two different roles, namely: as the sole electron acceptor material in the active-layer blend; and as additives to P3HT:PCBM based devices with the expectation that they might stabilize the morphology of the blend under thermal stress. In the initial stages of the work, HSS-12 was chosen as a probe as it had a reasonably high molecular weight and was soluble enough in the solvents used e.g., THF, to give

consistent films. For reasons of industrial relevancy, chlorinated solvents were avoided where possible.

In previous works it has been shown that the incorporation of oligomeric fullerenes as electron acceptors directly in the bulk heterojunction imparted substantial enhancements in thermal stability as compared to equivalent mono-fullerene devices, albeit with varying impact on initial device efficiency.[13,22] Here, the influence of increasing HSS-12 on the performance of P3HT:PCBM devices is investigated. Devices were made with the architecture: ITO/ZnO/P3HT:PCBM:HSS-12/PEDOT:PSS/Ag, in which PCBM was systematically substituted for HSS-12 while maintaining a constant ratio between fullerene content and P3HT. Figure 1 shows the typical J-V curves achieved as a function of the fullerene mix employed.
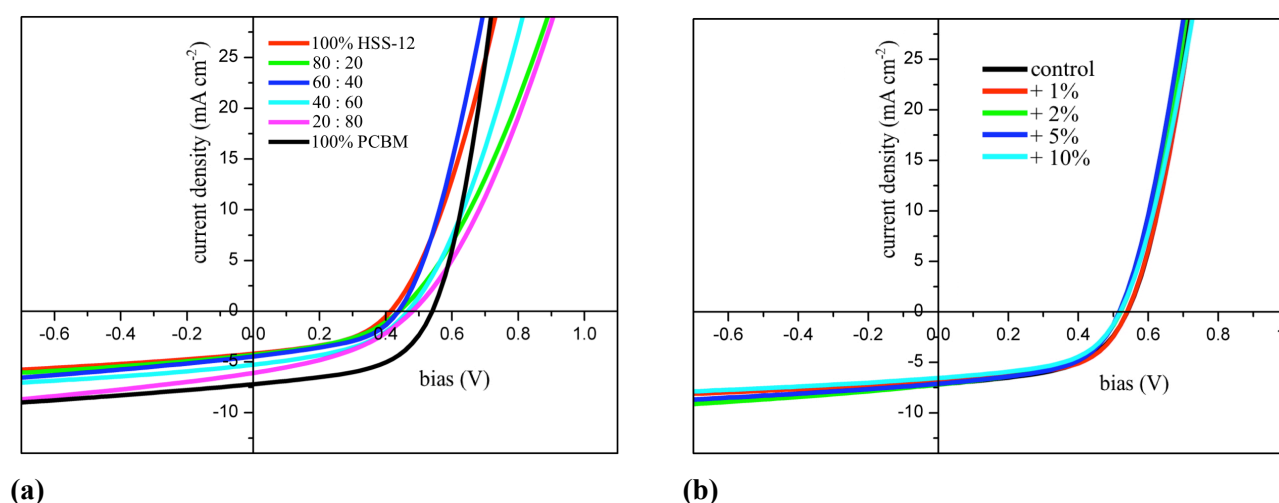

(a)   **(b)**

Figure 1. (a and b) *J-V* curves for OPV cells using high and low level loads of HSS-12 in blends with PCBM and P3HT.

Binary P3HT:PCBM and ternary P3HT:PCBM:HSS-12 devices achieved power conversion efficiencies (PCEs) of 1.85% and 1.8%, respectively (see Figures S1 & 2 for additional details). On increasing amounts of HHS-12 from 0 to 10% in a P3HT:HSS-12:PCBM ternary system, as shown in Figure 1b, the PCE started to decrease at amounts greater than 5% due to a drop in current density. This can most likely be explained by a negative effect on the morphology of the mixture. HSS-12 itself does not participate in charge extraction due to a large offset in acceptor LUMO levels (0.4 eV) hindering transfer of electrons from PCBM to HSS-12. However, there is no S-curve, which would suggest that the active layers retain reasonably homogeneous structures at the interfaces.

It is known that SACAP-based PFs,[13,31b] and oligomers of PCBM formed from ATRAP reactions,[22] can provide a strong stabilising effect against thermal degradation when used at low concentrations in OPV active-layers. Here, we similarly explore a simple C_{60}-based PFBMB as a stabilising additive.

Up to this point, HSS-12 has been used as a probe to survey the possible use of PFBMBs in inverted OPV cells. With this data in hand, we looked at the full set of the five PFBMBs shown in Table 1, each with a different lateral chain, to consider their impact on the nano-morphology of the active-layer and see how PFBMBs might operate as stabilisers in OPV devices.

In this study, each of the PFBMB's, reported above, were incorporated into P3HT:PCBM active layer blends as an additive at a loading of 10wt%. This fraction, while relatively high, was chosen to amplify the behaviour of PFBMB in the device thereby making characterisation more facile.
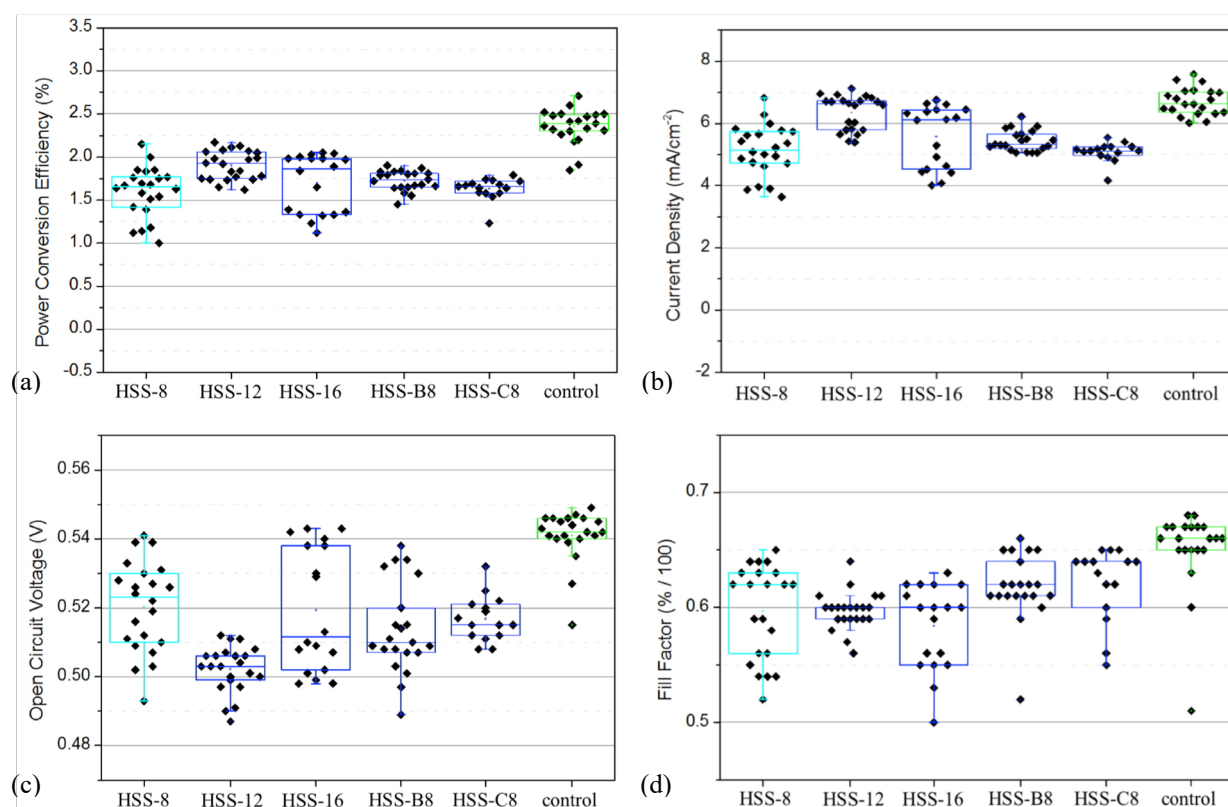

Figure 2. Variations in photovoltaic characteristics with different PFBMB additives, all at 10% w/w with respect to PCBM: (a) PCE; (b) J_{sc}; (c) V_{oc}; and (d) FF.

Figure 2 shows the initial device characteristics/performance for each of the five PFBMBs at 10wt%. Each PFBMB device achieved an average efficiency of between 1.7 and 2.0%. In contrast, PCBM control devices achieved an initial PCE of ~2.4% due to a comparably higher observed V_{OC}, J_{SC} and FF. All devices were then subjected to 140 °C in an inert environment to determine the extent of any stabilising effect of the PFBMBs on device performance under thermal stress. Figure 3 shows the change in PCEs with time. After a short period of stable behaviour, the PCBM control devices exhibit an initial steep decay followed by a relatively slower drop in performance up to 5 h. In contrast, the PFBMB containing blends exhibit a very rapid drop in PCE within 15 minutes of

annealing followed by a much slower decay appearing to plateau at longer timescales. All drops in PCEs are mainly driven by reductions in current extraction. Interestingly, unlike other PFs, here we see no stabilising effect from the PFBMB acceptors. Indeed, the rapid onset of degradation at short time scales is indicative of aggregation throughout the active layer. Notably though, it is apparent that HSS-12 and HSS-16 are the least unstable of the PFs, and that their long side chains are enhancing material stabilities. This might well be due to dissipation of vibrational (thermal) energy.
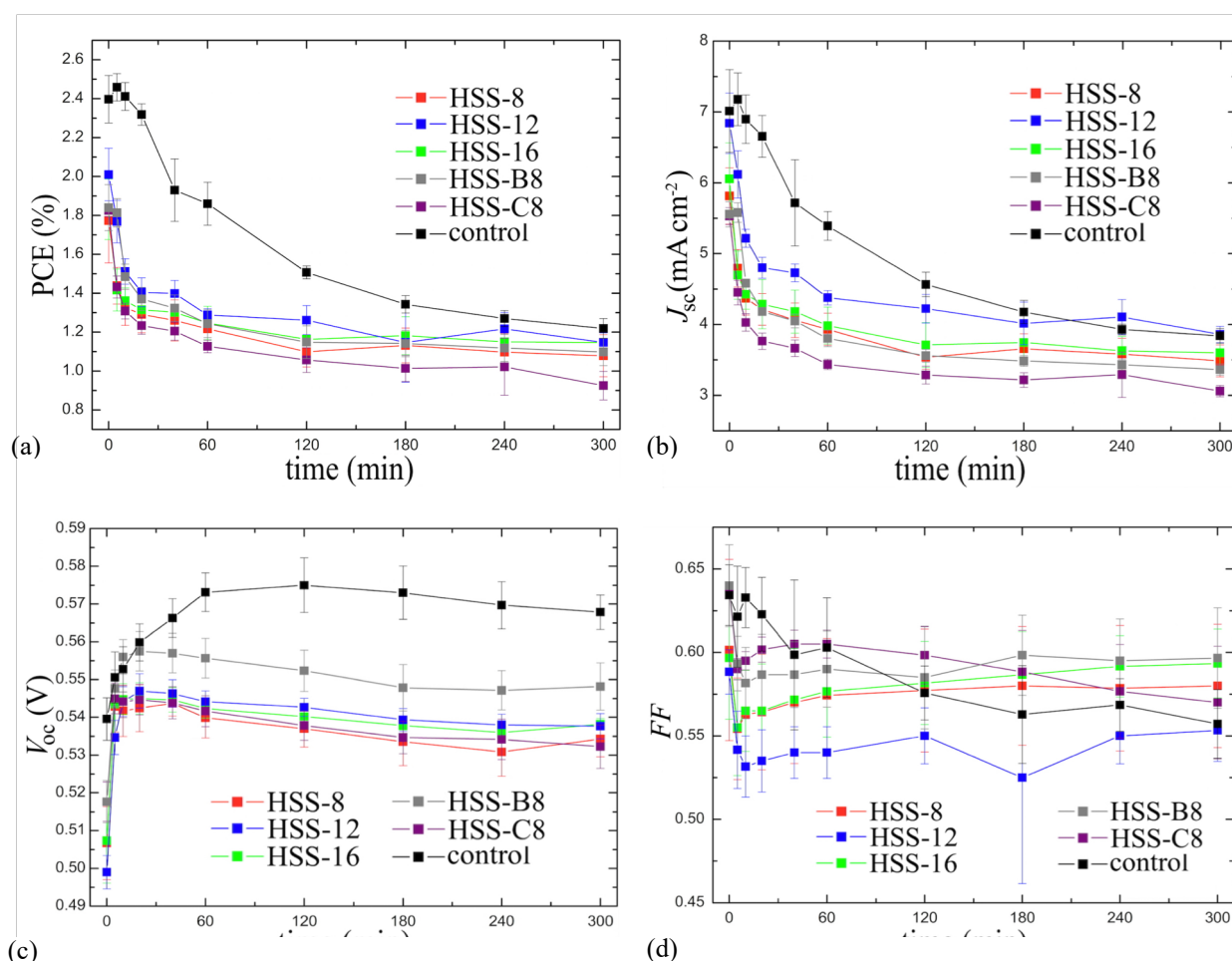

Figure 3. Variations in photovoltaic characteristics with accelerated aging by annealing at 140 ˚C: (a) PCE; (b) J_{sc}; (c) V_{oc}; and (d) FF.

To better understand the underlying processes, the thermal, photochemical and photo-oxidation degradation of HSS-12 both alone and in blends was studied. As mentioned in the introduction, thermal effects most easily introduce molecular migration and phase separation. Photochemical degradation, however, can be considered as a reaction capable of changing both the morphology and the chemical structure of p- and n-type materials.[35] For example, it is known that fullerene-derivatives are light-sensitive, and can undergo dimerization when irradiated with UV-visible light.[36] Finally, thermo- and photo-oxidation induce OPV-performance losses by changing the

7

electronic structures. As it has been shown that the products from thermo-oxidation are similar to those issuing from photo-oxidation,[37] only the latter is studied here.

2.3 Thermal Degradation of PFBMBs Alone and in Blends with P3HT:PCBM

2.3.1 Thermal Degradation of PFBMB Alone

HSS-12 thin-films on ITO/glass substrates were prepared from *o*-xylene solutions using Doctor-Blade techniques to be around 150-200 nm thick. The SI gives the experimental details of this process. Films were then heated at either 85, 140 or 200 ˚C for 5 h under nitrogen. UV-visible spectroscopy was used to follow the evolution of the absorption characteristics of each film. Figure 4a shows the spectra of the initial solid state films of HSS-12 compared against the spectra of HSS-12 solutions in toluene or THF:toluene (99.1 vol%), while Figures 4b-d show the evolution of the absorptions of the films with time.
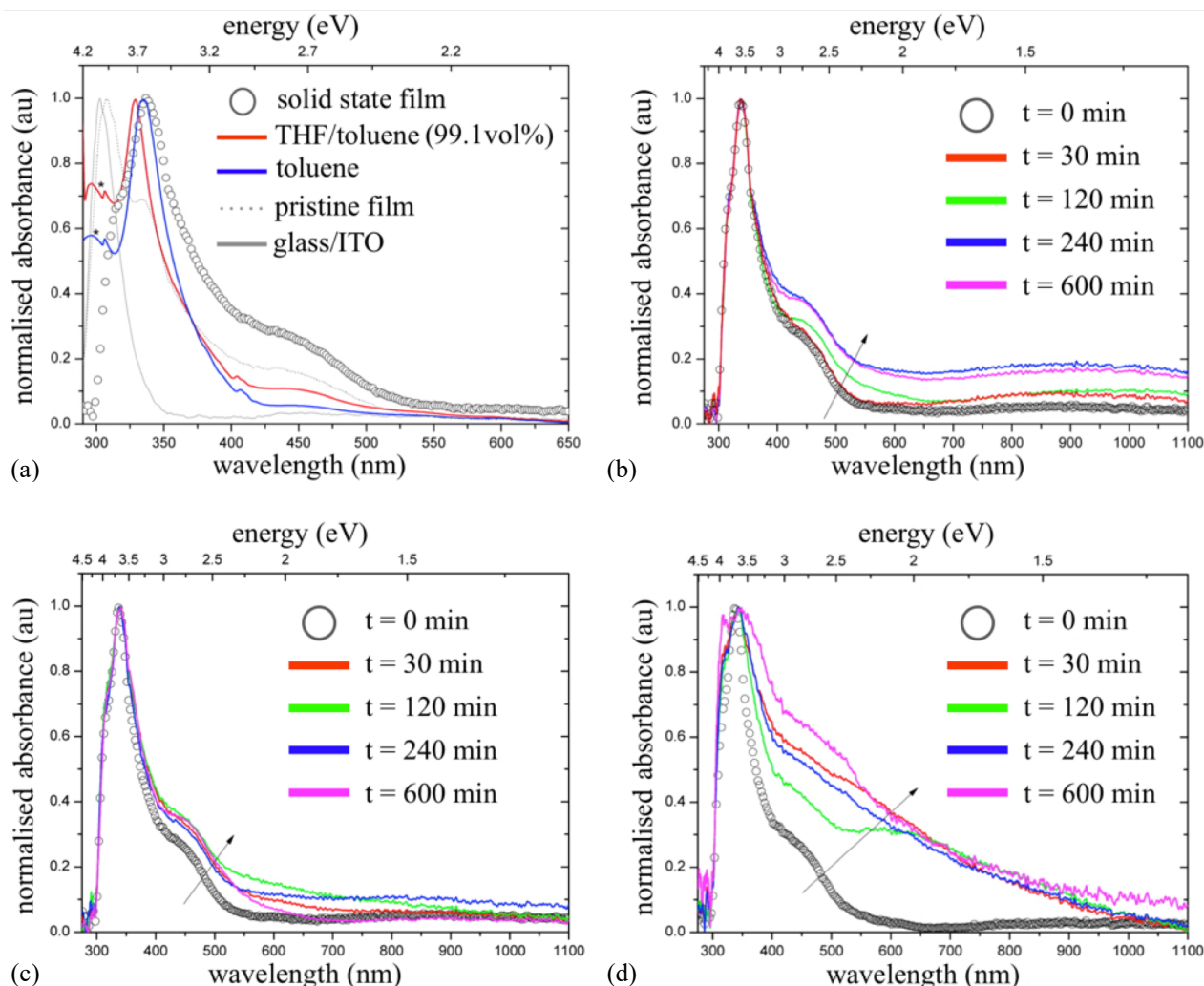
Figure 4. UV-visible spectra of: (a) HSS-12 as a non-annealed thin film, and of solutions of HSS-12 in toluene or in THF:toluene mixtures; and of HSS-12 thin films undergoing heating at: (b) 85 ˚C; (c) 140 ˚C and (d) 200 ˚C. Please note that: the pristine film is the same as the solid state film but with ITO and glass contributions removed; films are normalised around 311 nm to remove differences arising from films thicknesses, hence the use of arbitrary units (au); the solid state spectrum has been subtracted from the ITO/glass transitions; and the small stars in (a) indicate a small peak arising from an auto-change in the equipment's light source.

In Figure 4a one can see that the absorptions of HSS-12 in the solid state are very similar to those arising from its solutions. In all cases, there are strong, broad-band absorptions at 450 nm diagnostically associated with the dimethylene links to the fullerene sphere.[38-41] Similarly, the bands from around 300 to 420 nm, associated with internal transitions of the C_{60} moieties, are unchanged, although slightly broadened in the solid state, perhaps due to slight distortions in the C_{60} groups caused by proximity and steric effects. Nevertheless, given the absence of a bathochromic shift, it is possible to state that the dominant quality of the system is that HSS-12 behaves similarly in the solid state and in solution. This inference is supported by the fact that there is no band over 600 nm, indicative of an absence of aggregation.

Turning to Figures 4b-d, the evolution of the spectra is shown with respect to time and different heating temperatures. Films heated at 85 ˚C and 140 ˚C show quite similar changes, however, that heated at 200 ˚C exhibits a different profile. The bands around 350 nm associated with the C_{60} moieties slightly broaden for the samples at 85 ˚C and 140 ˚C and greatly widens for the sample heated at 200 ˚C. For the band at 450 nm there is a broadening in all cases that is hugely enhanced at 200 ˚C. Indeed at 200 ˚C, there is a fast abrupt change. This and the aforementioned broadening of the peak at 350 nm would tend to suggest that the system is undergoing some dynamic crosslinking process involving the breaking and reformation of comonomer-fullerene bonds.

At the lower temperatures, over longer periods of time, and at 200 ˚C, within 30 min, we also see the formation of a band between 500 and 700 nm which hints at the formation of conjugated by-products and asymmetric modification of the C_{60} sphere, for example via the formation of tetramers and seximers. Above 700 nm there is also a strong formation of wide, low intensity bands. This process also occurs to some extent at lower temperatures, but is particularly pronounced between 700 and 1000 nm at 200 ˚C. This indicates the formation of small aggregates which are absorbing light resonantly. As they increase in size though, the absorption intensity is overwhelmed by the light scattering intensity, which is λ^{-4} dependent. This would explain the broad absorption seen here and would confirm the formation of large particles through a process of crosslinking via rupturing of the fullerene-dimethylene bond, crystallisation and/or dimerisation of fullerenes, or etherification through reactions with trace oxygen. A liberation of fullerene from the PFBMBs would also explain the reduced V_{oc}s of the devices by way of C_{60} having a much lower LUMO (*ca.* -4.5 eV)[42] and with its dimers, acting as electron traps to reduce the current flow.

The effect of absorption in the lower energy part of the spectrum is a non-resonant effect and it has been effectively used by Tan *et al.*[43] to quantify the quality of carbon nanotube dispersions. We propose here an adaptation of their method to analyse the aggregation of fullerenes. In their work, the quality of the nanotube dispersion is dependent on how they disaggregate in a solution containing a surfactant; this has a direct impact on the band-width of the non-resonant background and on the band-width of the molecular resonant transitions. Their absorbance and scattering behaviour can thus be summarised using:

$$RR = \frac{\sum_{spectrum} A(\lambda,t)d\lambda}{\sum_{spectrum} NRB(\lambda,t)d\lambda}$$

eqn (1)

in which *RR* is the resonance ratio, $A(\lambda,t)$ is the temporal dependence of the resonant bands of the absorption spectra and $NRB(\lambda,t)$ is the temporal dependence of the non-resonant background of the absorption spectra.

For our system, we have fitted the UV spectrum of HSS-12 with six Gaussian functions. Three of these fit the C_{60} internal transitions at 312, 334 and 360 nm. The fourth, centred at 418 nm, is used to fit the band associated with fullerene resonances arising from a dimethylene attack. The final two are used to fit the non-resonant background. Figure S3 in the SI shows how these functions fold inside the HSS-12 spectrum. Positing these ranges into eqn (1) gives us:

$$RR = \left. \frac{\sum_{spectrum} A(\lambda,t)d\lambda}{\sum_{spectrum} NRB(\lambda,t)d\lambda} \right|_{t}$$

eqn (2)

The need of four Gaussian functions to fit the resonance bands can be determined by the analysis of the spectrum using the 2nd and 4th derivatives. It is possible to readily identify the difference between these two classes of Gaussian functions by way of their full width at half maximum (FWHM). As observable in Figure S3, for the first four functions, an FWHM of the order of 10-25 nm is reasonable, whereas for the latter two, it increases to greater than 100 nm.

In addition to the parameter RR, one can quantify the increase in the non-resonant scattering background signal by simply comparing the integral density of absorbed photons Φ, i.e.:

$$\Phi = \int_{spectrum} A(\lambda,t) - \int_{spectrum} A(\lambda,t=0)$$

eqn (3)

This is based on the assumption that the resonance bands are not influenced by any aggregation process that may take place and the only difference in the time evolution of the spectrum is the increase in scattered light. One has to pay close attention to the fact that RR and Φ will behave in the same way only if the observed changes are not electronic (shifts, decrease/increase of absorption coefficient) but solely based on aggregation. In the case of RR, this is assured by using the Gaussian curves parameters of the first four bands, which are resonant, as a constraint in the fit of the spectra of time evolution. This leaves just two Gaussian functions to fit the non-resonant background.

The upshot of these calculations can be seen in Figure 5, which shows the changes in RR and Φ with temperature and time. Note, the inverse of RR is shown so that it is more easily comparable with Φ.
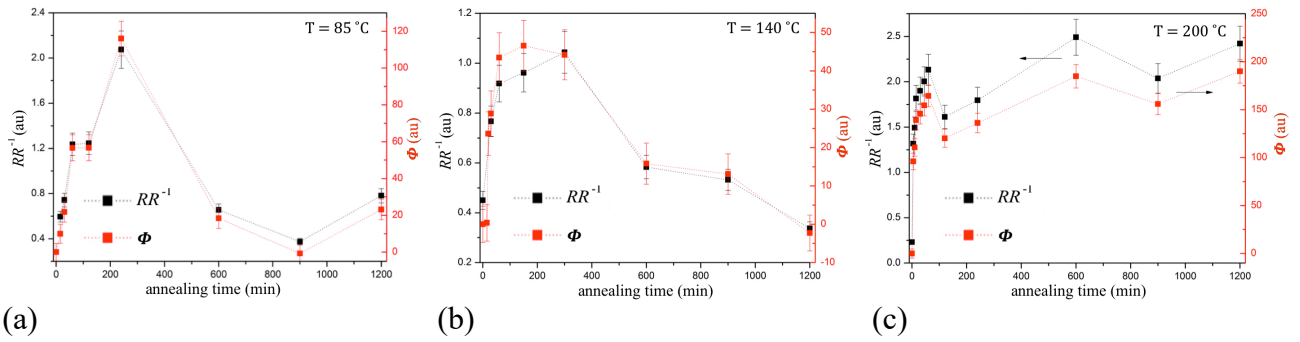
Figure 5. Evolution of *RR* and *Φ* with time for films annealed at (a) 85 ˚C; (b) 140 ˚C and, (c) 200 ˚C. Note: *RR* is presented as RR^{-1} to facilitate comparison with *Φ*. It can thus be interpreted such that as it increases it indicates a decreasing degree of aggregation in the bulk. Lines are guides to the eye.

The curves in Figure 5 can be interpreted as follows. An increase in *Φ* indicates an increase in the summed photons with respect to that at $t = 0$, and this increase is directly related to an increase in the non-resonant background resulting from aggregation effects. A decrease in *RR*, or rather an increase in RR^{-1}, indicates a decrease in the homogeneity of the fullerene dispersed within the sample. With this in hand we can see that at 85 ˚C, there is a fast decrease in homogeneity within the first 300 min, but after this there is little change. A similar profile is observed at 140 ˚C, although some changes continue after 300 min. At 200 ˚C, however, there is a much more considerable change in the fullerene homogeneity that continues with time. This would again suggest that there is some underlying chemistry involved at these temperatures which is impacting the structure of the material.

This data can be compared with that found through AFM characterisations. Figure 6 shows the effect of heating on the surface of the film and with the scales gives a visual indication of the changes in the surface heights. After 4 h at 85 ˚C we see an increase in the number of aggregates, and in the route mean square (RMS) roughness, to around 17 nm with respect to the pristine and relatively smooth HSS-12. Not shown in the images, but interesting to note is that on continued heating the RMS roughness increased to around 30 nm after 10 h, and then decreased to only a few nm after 15 h. As to why this happens remains unclear. At 140 ˚C, the harder islets take on a more crystalline form, suggesting the presence of fullerene. Also suggesting this formation of crystals, the RMS roughness has also increased to around 80 nm. Still at 140 ˚C, but after a longer time (the images g-i are after 5 h), these crystals seem to have disappeared, but the surface is now completely disorganised, although the RMS roughness has little changed at around 70 nm. On moving to 200 ˚C, over relatively short time periods (images j-l were made after 1 h of heating), we can again see the highly aggregative structure appearing, with a complete loss of lateral homogeneity, and an increase in the RMS roughness to 120 nm. This value does not increase much more after ten hours.

To sum, these results closely corroborate those from the UV-visible characterisations; that there is a time and temperature dependency of the formation of aggregates, and that a high

temperature drives this process. At lower temperatures i.e., around 85 ˚C the process is slower and less catastrophic.
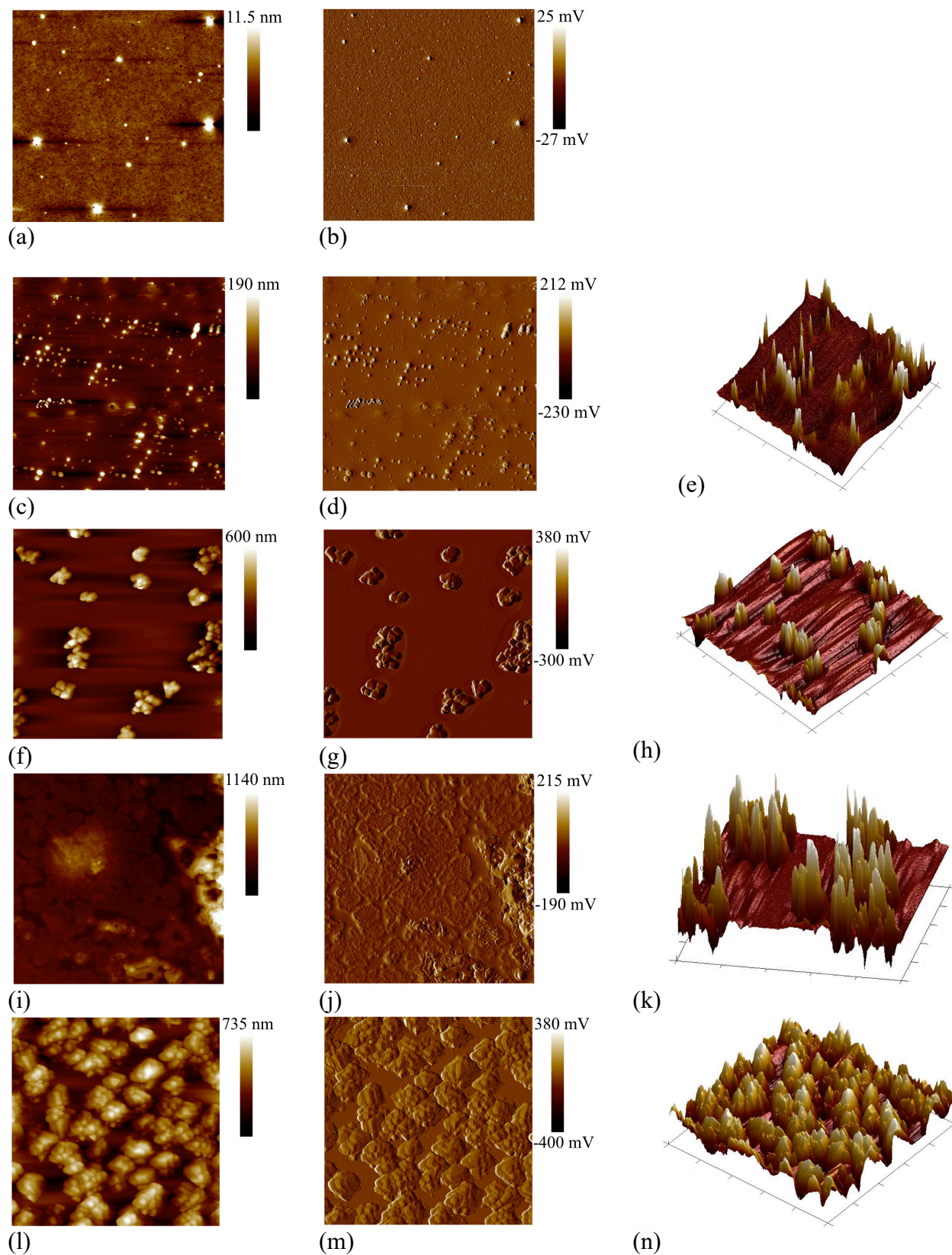

Figure 6. From left to right, representative AFM height, amplitude and reconstructed 3D images of HSS-12 films show the effect of thermal treatments under nitrogen, from top row to bottom row, at:

(a,b) pristine films (d-f) 85 ˚C for 240 min; (g-i) 140 ˚C for 60 min; (j-l) 140 ˚C for 300 min; and (j-l) 200 ˚C for 60 min. Please note that images d-f are are all 20 μm wide, while all other images are 10 μm wide.

X-ray photoelectron spectroscopy (XPS) was used to infer the chemical structural changes induced by the thermal treatments. The same batch of HSS-12 films submitted to the prior characterisations were characterised. The spectra indicated that there was 92.0% carbon and 5.8% oxygen present (Figure S4 in the SI). This relative ratio implies a presence of oxygen which is three times higher than would be expected from the structure of HSS-12. It is well understood that fullerene, especially C_{60},[44] reacts readily with oxygen to form ethers,[45] and even short exposures to air during the film formation and synthesis would explain this.

On annealing there is no major change in the C1s peak except for a broadening for increasing annealing times and/or temperatures, as indicated in Figure S5. A slight change in the position and intensity of shake up features might be visible in Figure S5, which could be due to a change of the electronic structure (e.g. a variation of the HOMO-LUMO separation) or due to the presence of additional oxidized carbon species contributing to the C1s photoelectron spectrum, which cannot be completely ruled out, even if the annealing was carried out in nitrogen atmosphere.

2.3.2 Thermal Degradation of PFBMBs in Blends with P3HT:PCBM

We now turn to the degradation of the probe PFBMB, HSS-12, in a blend with P3HT and PCBM. Two blends were prepared, one of P3HT:PCBM in a 1:1 ratio, and another with P3HT:PCBM:HSS-12, in the respective ratio 5:4:1 so that the HSS-12 made up 25% of the fullerene weight. Both were prepared using Doctor-Blade techniques from *o*-xylene solutions, as detailed in the SI, and annealed in the same manner as films of PFBMB alone.

Figure 7 shows the impact of thermal annealing on the absorption profiles of the blends with and without HSS-12. Figure 7 c also shows how the band at around 340 nm, associated with fullerene electronic transitions, decreases *more* rapidly for the blend with the HSS-12. This would tend to suggest a rapid phase segregation and consequent crystallization of PCBM molecules.
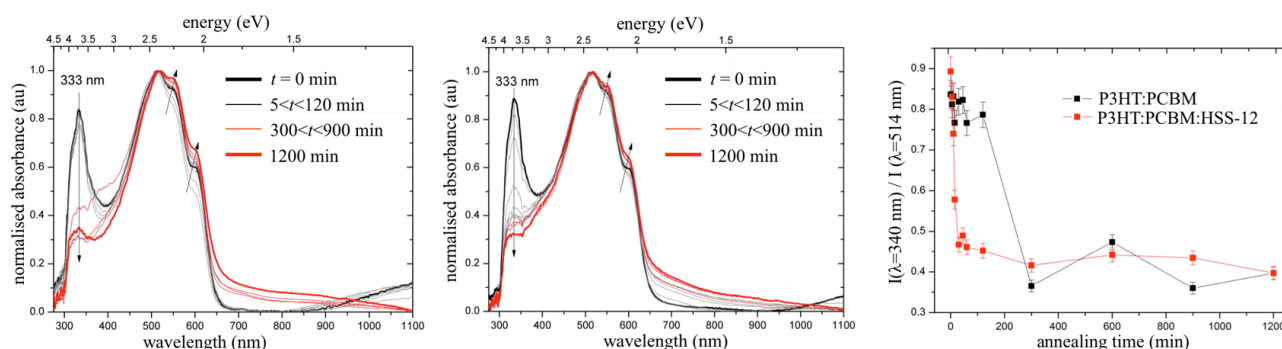
Figure 7. Optical behaviour of blends with thermal annealing at 140 ˚C under nitrogen for: (a) P3HT:PCBM blend alone; and (b) P3HT:PCBM:HSS-12 blend. The graph in (c) shows the evolution in the absorbance at 340 nm with respect to the steady absorbance at 514 nm for the same two samples.

This process can be observed in Figure 8 where one can see images for the pure P3HT:PCBM blend (left) compared against those for the P3HT:PCBM:HSS-12 blend (right). At t = 0, both samples are quite similar, however, with annealing at 140 ˚C, they become increasingly different, with a rapid and drastic formation of clusters in the case of the P3HT:PCBM:HSS-12 blend. This result is confirmed by the changes in the RMS roughness in that for P3HT:PCBM it stays quite stable (between 10 and 20 nm) while that of the blend with HSS-12 shows a sharp rise to ca 60 nm in the first 30 min, and continues increasing with time (Figure S6 in the SI). So, in effect, the HSS-12 does the opposite of what would be expected; it increases the speed of phase separation.

These results are confirmed by XPS analysis that was performed on the pristine and thermally annealed blends. For the P3HT:PCBM blend, as would be expected from prior work,[3b] the PCBM migrates vertically to the surface, as indicated by the decrease in the presence of sulfur due to P3HT and the increase in the concentration of oxygen associated with PCBM. However, in the P3HT:PCBM:HSS-12 blend, the concentration of sulfur remains relatively stable, while that of oxygen shows a slight, if unsteady, increase. These results are further details in Figure S7 and Table S1 in the SI. With the prior results, this would tend to suggest that the PCBM arising at the surface in P3HT:PCBM:HSS-12 blends leaves domains of P3HT present, and therefore does so in large, deep aggregates, much like icebergs, rather than taking on large areas of the surface.
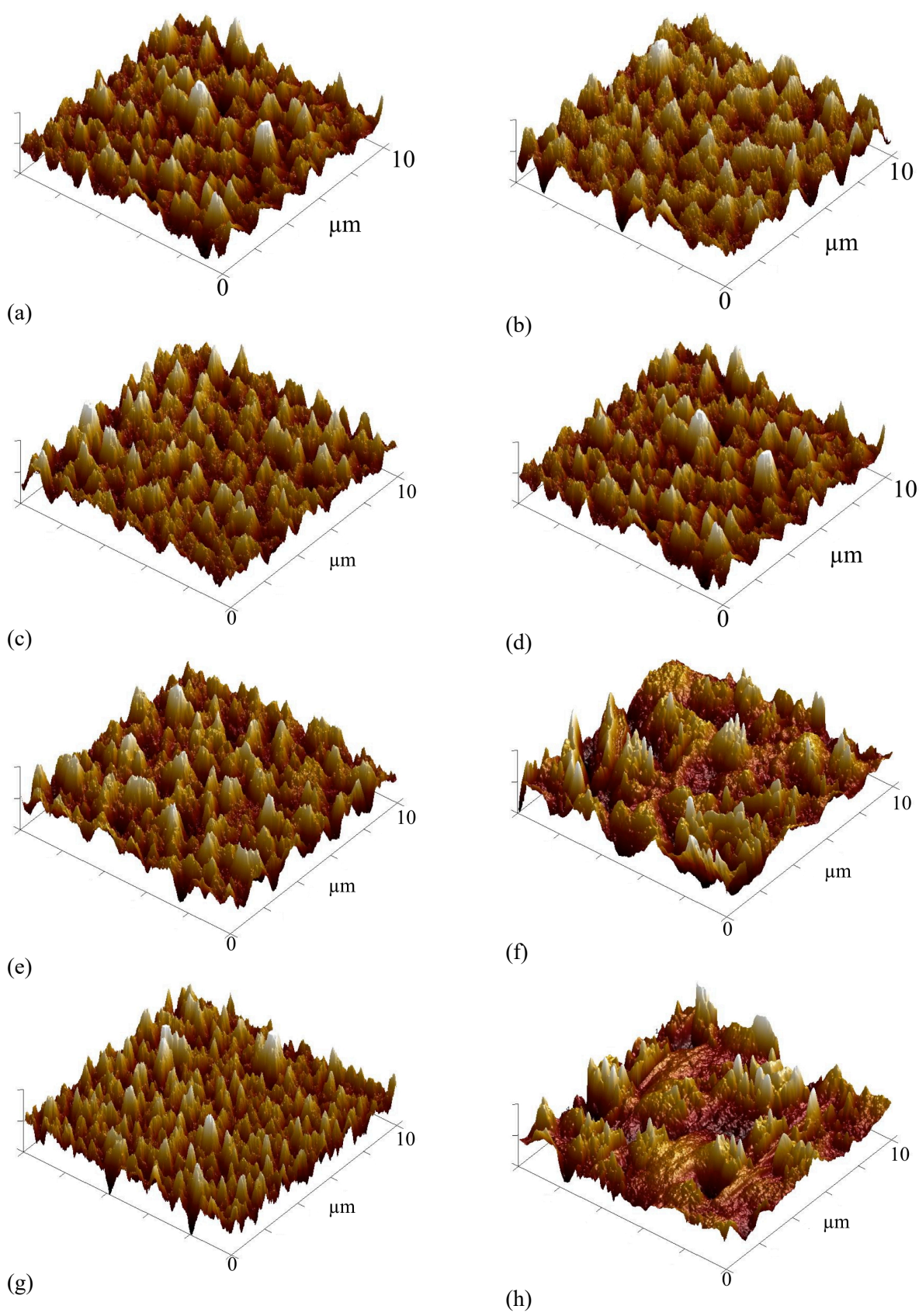
Figure 8. 3D AFM reconstructions showing the evolution of blend surfaces with annealing at 140 ˚C under nitrogen. On the left, P3HT:PCBM (a, c, e, g), and on the right P3HT:PCBM:HSS-12 (b, d, f, h), respectively recorded at t = 0, 30, 1220 and 300 min.

2.4 Photodegradation of PFBMBs Alone and in Blends with P3HT:PCBM

2.4.1 Photodegradation of PFBMB Alone

Again, HSS-12 was used as a probe to investigate and possible photo-degradative processes. Films of HSS-12 (prepared as detailed in the SI) were submitted to AM1.5 conditions under a nitrogen atmosphere. The evolution of the films was followed using UV-visible spectroscopy and XPS. The UV-visible data, collected in Figure 9, shows both the spectra and the changes in the *RR* and *Φ* parameters, as defined earlier in the text. With these results one can discern an initial phase, where t < 400 s, where the non-resonant background scattering decreases, and then rapidly increases to remain more or less constant for the rest of the experiment. This might indicate the presence of two processes, the first, possibly, where short range dimerisation occurs, and the second, where there is a formation of large clusters.
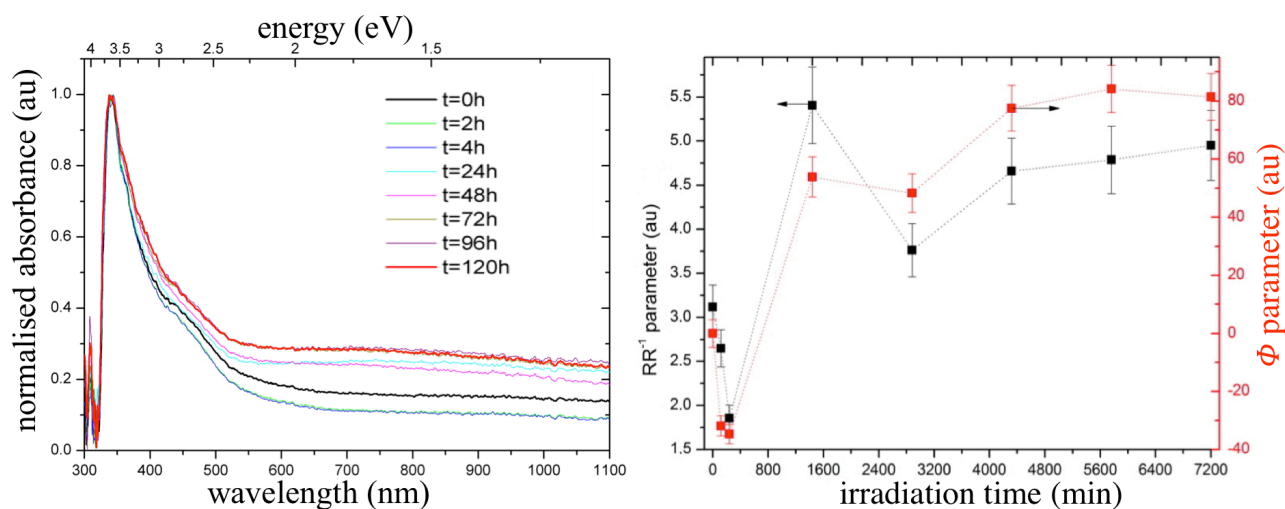

Figure 9. (a) Evolution with time of the UV-visible spectra of HSS-12 deposited on ITO/glass illuminated under AM1.5 conditions and under nitrogen. (b) Evolution with time of the *RR* and *Φ* parameters, defined in the main body of the text.

It is known that fullerene molecules tend to undergo dimerization with light irradiation under vacuum *via* a photochemical [2+2] cycloaddition reaction and this converts two intramolecular sp^2 double bonds in two intermolecular sp^3 single-bonds.[46] This process tends to be reversible with temperatures over 100 ˚C. Distler *et al*. have shown that this decreases electron mobility in the fullerene phase,[47] while Wong *et al*. showed that light exposure can limit morphological degradation by way of PCBM's capacity to photo-oligomerize.[48] Whereas these structures only involve two fullerene molecules, their concentration can increase in such way as to result in the formation of islands of aggregated material. Therefore it might be hypothesized that similar 2 + 2 additions can occur between fullerene's in the chain. However, one can also reason that the polymeric structure of

HSS-12 and the long alkyl chains should restrain such a process from taking place. Another possibility is the unzipping of HSS-12 during the thermal degradation process leading to C_{60} and, subsequently, its dimers.

In an attempt to further explore this, XPS characterisation of C1s peaks with increasing irradiation times under nitrogen atmospheres was performed. The increasing broadening of the peaks that affect the position of the first shake-up, indicate that the homogeneity of the surface and its electronic structure evolve with irradiation in an inert atmosphere. Comparing these values to the ones found for evaporated C_{60} (Gaussian width of 0.75 eV, first shake-up energy of 1.80 eV with a total contribution to the curve's components of 8.6%), one could say that the formation of something similar to free fullerene is occurring. An increased intensity of the first shake-up may indicate an increased number of sp^2 carbons, as discussed in reference 49. This could imply the formation of additional free C_{60} molecules. However, since oxidized carbon species are expected in the same energy range, a quantitative analysis is impossible. However, the similar peak shape of the C1s core level spectra as a function of the irradiation time in Figure S8 indicates the presence of fullerene-related molecules in all cases.

2.4.2 *Photodegradation of PFBMB in Blends with P3HT:PCBM*

The effect of HSS-12 on the morphology under AM1.5 conditions in an inert atmosphere was studied. Figure 10 shows the evolution of the UV-visible spectra for both systems for different exposure times, measured at the same point of the sample.
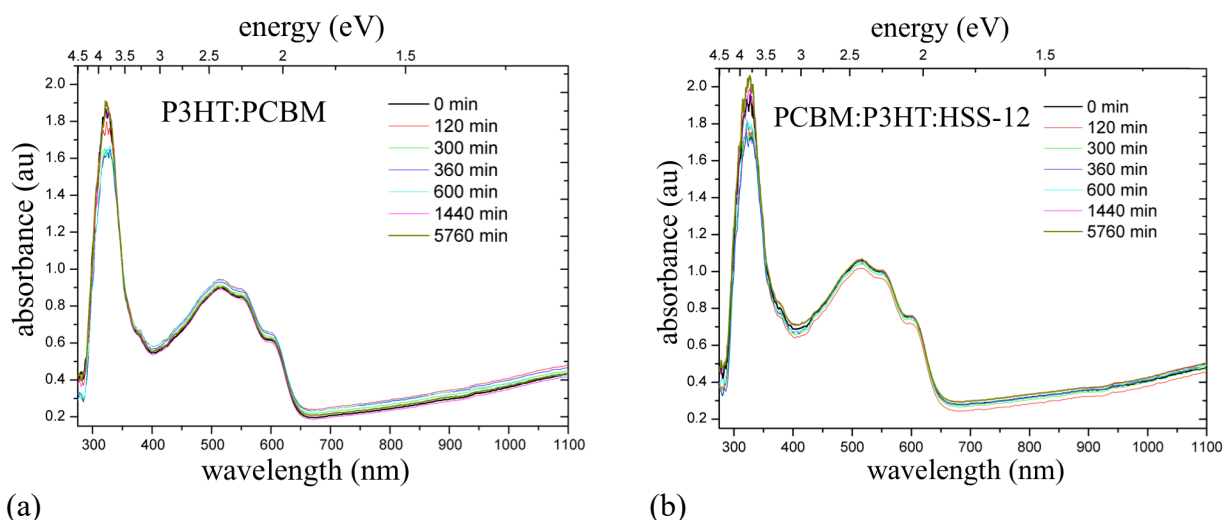

Figure 10. Evolution of UV-visible spectra with time for: (a) P3HT:PCBM (1:1 wt ratio) and; (b) P3HT:PCBM:HSS-12 (5:4:1 respective weight ratio).

From these spectra, one can see that the most sensitive region of the spectra is the fullerene absorption band around 340 nm, which initially decreases with time to regain its original position

after 1440 minutes or so. Distler *et al.*[47] identified increases of lower wavelength bands (320 nm and lower) with dimerisation, and it could be supposed that this decrease at 340 nm is due to a process from oligomers to dimers. The later increase is most likely due to the formation of crystalline states, which would also explain the increased scattering at higher wavelengths.

These results are further corroborated by those from AFM characterisations of films of P3HT:PCBM and P3HT:PCBM:HSS-12 that had been similarly illuminated under AM1.5 conditions and N_2 for 120 h (Figure S9). Their RMS roughnesses changed from being initially very similar, at 11 and 13 nm, to differentiate at 14 and 23 nm, respectively. In effect, P3HT:PCBM:HSS-12 is more sensitive to light irradiation than P3HT:PCBM alone. This was again confirmed by XPS analyses, carried out on films before and after 96 h of photo-degradative treatment (Table S2 in the SI). In both samples, the percentage of O increases, although much more in the sample with HSS-12, while the level of S stays the same with HSS-12 but decreases in that without it. This indicates that there is a migration of PCBM to the surface in both cases (carrying O), but that the P3HT, carrying S, is maintained at the surface in the mixture with HSS-12. This would tend to confirm that any fullerene that moves to the surface in the ternary mixture does so without occulting the polymer, i.e., it moves to form large clumps.

2.5 *Photo-oxidative Degradation of PFBMBs Alone and in Blends with P3HT:PCBM*

2.5.1 *Photo-oxidation Degradation of PFBMB Alone*

Films were exposed to AM1.5 irradiation under synthetic air using a Xe lamp, and their degradation accompanied by UV-visible, XPS and FT-IT spectroscopies. In the UV-visible spectra, there are two main bands that evolve with the process at around 340 and 430 nm associated with inner electronic transitions of C_{60} and characteristic transitions of C_{60} resulting from asymmetries from the polymerization attack, respectively. During the first 7 h of treatment, both bands decrease, after which the band at 340 nm stabilizes while that at 430 nm increases. This would suggest a fast release of C_{60} in a process of depolymerisation, followed by a secondary process of dimerisation of C_{60} through sigma-sigma bonds formation with light,[50] reactions with oxygen,[51] and/or some other additional reaction with the products of the depolymerization. Figures S10 and S11 showing this are in the SI.

C1s and O1s XPS peaks were also acquired during the degradation. In the C1s spectrum we find that the peak intensity around 288 eV increases (Figure S12), indicating, in contrast to the photodegradation under N_2 atmosphere, now clearly in the presence of oxygenated species visible at binding energies > 285 eV. The O1s broadens, indicating a formation of a wider variety of species (Figure S13). From Figure S12 it is visible that first lower oxidized carbon species are formed resulting in an increased intensity in the energy range between 285.5-287.5 eV, whereas higher

oxidized species (binding energy > 287.5 eV) appear after longer (>7h) exposure times. This may indicate that groups such as esters and carboxylic acids (high oxygen/carbon ratio and higher oxidation state) are likely to be predominant in the later stages of the photo-oxidation process. The early stages are likely to be dominated by the appearance of alcohols and formation of ether functions (low oxygen/carbon ration and lower oxidation state).

The C_{60} sphere and the comonomer will most likely not degrade at the same rates, and will also give rise to different degradation products. The degradation processes were thus accompanied by FTIR measurements, shown in Figure 11. These were performed by casting a film of HSS-12 on a KBr window and subjecting it to the same AM1.5 conditions under synthetic air for 96 h. The HSS-12 film gave rise to the characteristic bands of C_{60} (527, 576, 1182 and 1428 cm^{-1}),[50a,52,53] the -C-H vibrations characteristic of the alkyl chains (2849 and 2920 cm^{-1}), benzyl ring vibration (740 cm^{-1}), vibrations associated to the $-CH_2-CH_2-$ and ether vibrations (1375-1530 cm^{-1} and 1140-1240 cm^{-1} regions, respectively). Moreover, a wide ensemble of minor bands around 1015 cm^{-1} were found that might be associated with methylene link between the fullerene and the comonomer ($C_{60}-CH_2-$).
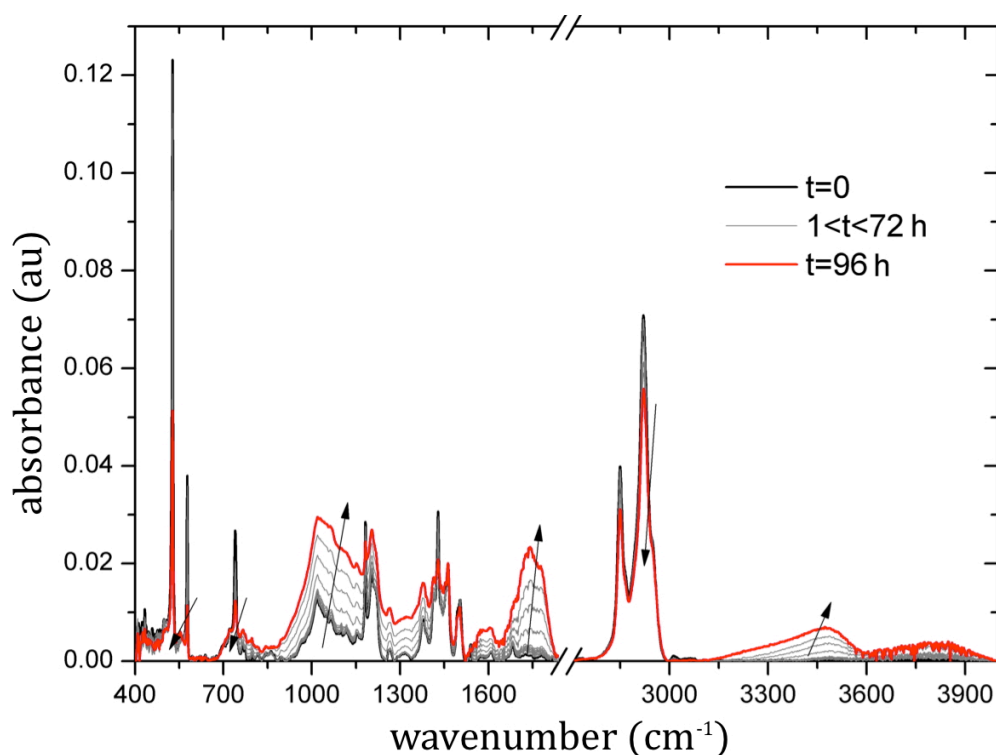

Figure 11. Evolution with time on the FTIR spectrum of HSS-12.

The evolution of these bands with respect to the initial state at t = 0 was followed. These were then fitted with Lorentzian functions for the vanishing bands and with the minimum number of

Gaussian functions for the rising bands. The collected rates of change for bands that underwent at least +/- 10% changes are collected in Figure 12 (the differential spectra are in the SI in Figure S14).
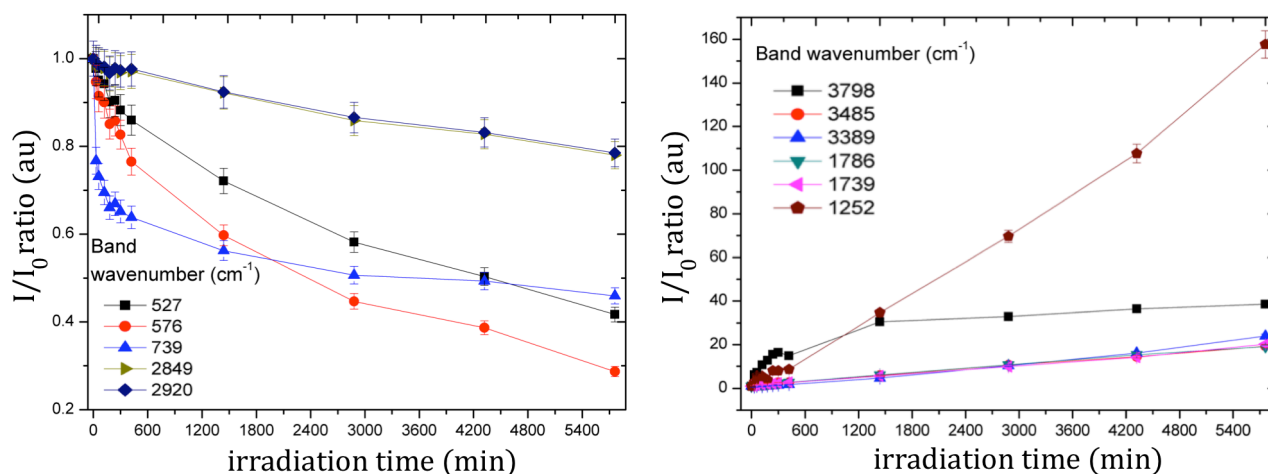

Figure 12. Photo-oxidation product formation: (a) decay rates for vanishing products; and (b) increasing rates for those being produced.

There are three main regions in terms of the FTIR signals and their associated degradation processes. The degradation of the C_{60} moiety is observed through decreases of bands at 527, 576, 1182 and 1428 cm^{-1} (the latter two are not shown in Figure 12 for the sake of clarity). The degradation of the comonomer ring can be followed through the evolution of the band at 739 cm^{-1}, and that of the lateral chains are indicated by changes in the bands at 2849 and 2920 cm^{-1}. It is worth noting that the latter two are coupled and arise from the same chemical group. Similarly, it is worth noting that for times below 7 h, the comonomer benzyl ring has a band at 739 cm^{-1} which decreases in intensity more quickly than all others. This would suggest that if there is a depolymerisation reaction, then it is occurring faster than photo-oxidations.

In the group of bands that rise, we find that there are: C=O vibrations (associated with esters, ketones, carboxylic acids, anhydrides and aromatic esters) appearing at 1785 and 1739 cm^{-1}; C-O vibrations associated with alcohols appearing at 1175 cm^{-1} (tertiary) and 1060 cm^{-1} (primary); other bands assigned to C-O bonds appearing at 1358 and 1251 cm^{-1}; and O-H bands associated with alcohols and carboxylic acids at 3389, 3484 and 3797 cm^{-1}. There are also bands appearing at 1595 cm^{-1} in the C-C neighbourhood from C-O or C=O vibrations. For those bands appearing at 1785 and 1739 cm^{-1}, it is most likely that they arise from the oxidation of C_{60}, given their proximity to bands found for C_{60} and PCBM photo-oxidation,[37] the agreement with prior work[54] and the aforementioned XPS data. The degradation of the lateral chains has been well characterised elsewhere and is based on the radical abstraction of lateral hydrogen chains.[10,35,55,56]

Returning to the fast degradation of the comonomer, we should note that it is very difficult to separate by FTIR alone the contributions of photo-oxidation products coming from the attacked

fullerene or the aromatic ring of the comonomer. Moreover, the band associated to the comonomer-C_{60} bond vibration (expected between 900-1100 cm^{-1}) should be altered if an underlying, concomitant depolymerization process occurs. Such a process would be expected to affect the affinity of the system to oxygen and might explain why the degradation process is generally fast.

2.5.2 *Photo-oxidation of PFBMB in Blends with P3HT:PCBM*

For the photo-oxidation studies of the P3HT:PCBM:HSS-12 blend, only the UV-visible technique was used. This method was chosen as the identification of the photo-oxidation products of P3HT, P3HT:PCBM and HSS-12 have already been performed. For the first two, the works of Chambon *et al*.[37] Sai *et al*.,[55] Manceau *et al*.,[57] and Hintz *et al*.[58,59] among others should be extensively considered. Again, here, photo-oxidation experiments were performed under AM1.5 conditions in synthetic air, using the same procedure as for the HSS-12 sample given above.

The UV-spectra for both systems, P3HT:PCBM and P3HT:PCBM:HSS-12, show no significant differences in their absorptions; both decrease slowly with time over the 96 h of characterisation (See Figures S15 and S16). This may simply be due to the radical scavenging properties of the fullerenes that dominate the slowing of polymer degradation, regardless of whether or not the fullerene is in a polymer chain.

2.6 *Depolymerisation of PFBMB*

The above results indicate that there are two processes; a rapid formation of small, highly crystallisable molecules and then a subsequent, slower reaction forming new products. The first process is faster than the photo-degradative and oxidation processes occurring at the fullerene. If the polymeric structure of the PFBMB were preserved, one would expect a better stability against thermal and light treatments.

Considering the literature, we find that several reports have indicated that the incorporation of pristine C_{60} to polymeric matrices has a retarding effect with respect the host polymer's thermo-oxidative degradation.[60] This is not a surprise given that these processes are radically initiated and C_{60} is a radical scavenger.[61,62] However, in the case of polymers joined to C_{60}, such as in C_{60}-polymer stars where the polymer is polystyrene or polyisoprene,[63] when covalently bonded, thermogravimetric measurements (TGA) indicated that fullerene release could be detected at relatively low temperatures and that the polymer-C_{60} bond, especially when that of a methylene link, is rather weak.[64-69] In particular, 6-*star*-polystyrene-*v*-fullerene and 6-*star*-polyisoprene-*v*-fullerene showed that a continuous release of the lateral arms attached to the fullerene moiety could be detected in solution at around 100 ˚C.[63,70] Pantazis *et al*. deduced that the bond cleavage-formation on the C_{60} sphere is

based on a dynamic equilibrium and the presented arguments that the rate of degradation depended on purification processes, reducing the quantity of available comonomers, shifting the equilibrium towards the reagents.[63]

Thus in the light of the results and the consideration of the literature, a hypothesis for a possible reaction is shown in Figure 13.
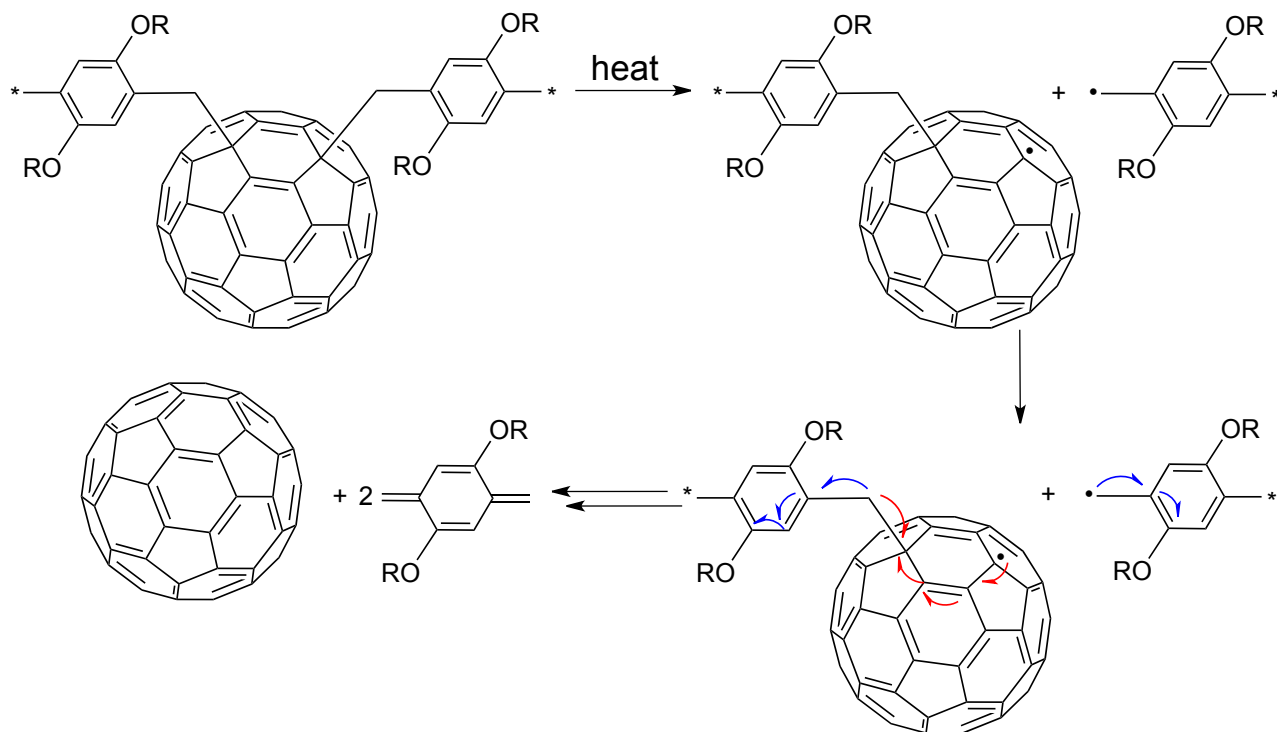

Figure 13. Scheme proposed for the depolymerization reaction and used for the calculation of energies.

In this process, a homolytic cleavage between the comonomer and the fullerene would lead to the formation of two radical pairs, one localized on the fullerene sphere and the other located on the CH$_2$ group of the comonomer. It is reasonable to expect that the delocalization of the benzyl-type radicals on the aromatic cycle is straightforward and this would lead to the destabilization of the bond in β position to the first cleavage. This having happened, both radicals are now in a closed-shell configuration, thereby gaining overall stability. The resulting *p*-quinodimethane would be expected to rapidly react, either with itself to form oligo(phenylene vinylene), with fullerene to form new sigma-bonded species, or oxygen in accelerated (photo-)oxidative reactions. It would also be expected that the fullerene goes on to dimerize. We now look more specifically at the thermal and light assisted degradations of PFBMBs in the light of this hypothesis.

2.6.1   *Thermally-induced Depolymerization of PFBMBs*

We calculated the bond dissociation energies of the fullerene-comonomer link by different ground- and excited-state molecular methodologies. For a B3LYP/6-31G** ground-state molecular geometry, the coordinate reaction of the bond dissociation was scanned and the energy point evaluations along their Morse-like potential fit curve are presented in Figure S17 in the SI.

This very low bond-dissociation energy range (20 to 50 kcal mol^{-1}, with an average energy of 39.65 kcal mol^{-1}) for the fullerene-comonomer link is in agreement with experimental results obtained for 2-, 4- and 6-arms (PS)$_6$C$_{60}$ materials, measured under TGA conditions (45.45 kcal mol^{-1}).[65] When only the initial (bonded) and final (dissociated) states are calculated, a scan of the reaction coordinate corroborates this value by giving 39.65 kcal mol^{-1}. This is only possible as no rearrangement reaction can take place during the cleavage.

Mechanistically, the thermal energy induces a breaking of the fullerene-comonomer link leaving behind two radicals each one found in one product. Considering the results found by Audouin *et al*.[69] the coupling of two radicals born by the C$_{60}$ is unlikely because of the steric hindrance due to the attached chains. It is also known that C$_{60}$-C$_{60}$ bonds are easily broken.[71] The authors proposed that on heating the radicals probably reacted with impurities. Unlike their system though, our system is based on an intimate alternating copolymer of C$_{60}$ and comonomer, and therefore it is possible to calculate the bond dissociation energy involved in the cleavage of the opposing opposite fullerene-comonomer bond in the second step in Scheme 1.

This mechanism relies on the fact that, once formed, both radicals delocalize in the surrounding molecules, and recombine readily with others formed nearby, thus leaving a closed-shell configuration with an overall energy gain. The calculated bond dissociation energy for the 1st cleavage is of the order of $\sim$ 55 kcal mol^{-1} (Figure S18 gives more details). Once the first cleavage has taken place, we calculate that the second requires an energy of around 14 kcal mol^{-1}. This exceptionally low energy indicates that once the first bond is cleaved all other bonds should cleave giving rise to the same mechanism, reducing the energetic barrier needed to start the degradation. Interestingly this mechanism proposes that there is a facile a rapid formation of C$_{60}$ and *p*-quinodimethane products. The former would explain the formation of crystals in the studies above, while the latter are known to be unstable and are typically considered as intermediates in the formation of larger species, for example, poly(phenylene vinylene) and [2.2]-1,4-cyclophane, or with C$_{60}$ to form small molecular bridged species (their structures are shown in Figure S19).[72]

While explaining the results observed in the characterisations set out here, this process of degradation may also explain why one cannot obtain high molecular weights with ATRAP. The formation-cleavage of the fullerene-comonomer link should follow an equilibrium that is easily shifted towards the reagents. Furthermore, it explains the surprising formation of crystalline structures

seen in prior work with PFBMBs, which may have arisen from small molecularly modified C_{60} (arising post-reaction as detailed below) or C_{60} itself formed *in-situ*.[73]

In an attempt to gain more evidence for the mechanism, we performed NMR experiments on a sample of HSS-12 heated at 100 ˚C in d_8-toluene under nitrogen (Figures S20-22, SI). First, there is no increase in groups, indicating no hydrogen abstraction by *p*-quinodimethane. Second, we see that a large proportion of the starting material (HSS-12) remains. However, multiplets do form at around 7.45, 7.25 ppm and a doublet forms at 6.55 ppm, indicating the presence of short aromatic species. Also there is a range of peaks formed at around 3 to 4 ppm, but no observable change in peaks around 5-6 ppm. These results would suggest that while oligo(phenylene vinylene)s might be formed, they are definitely not a majority species; the presence of peaks between 3 and 4 ppm would suggest the presence of alkyl groups in highly constrained positions, such as those on cyclophanes and on C_{60}-adducts. Given the radical loving nature of C_{60}, that the formed C_{60} quenches reactive *p*-quinodimethane to give such adducts would not seem far removed.

2.6.2 *Light-induced Depolymerization of PFBMBs*

Besides the thermally-induced bond cleavage of fullerene-comonomer bond, based on the results provided from the photochemical degradation tests, one can also consider a light-induced mechanism of bond cleavage. This hypothesis is also motivated by dissociation curves (Figure S17, SI) for which the energy of dissociation on the first excited state is decreased by a factor of at least 2. To go deeper in this hypothesis, we have optimized geometries of hydrogen-passivated comonomers in the ground singlet (S_0), first excited singlet (S_1) and first excited triplet (T_1) states. The calculation was performed within the B3LYP/6-31G**/RIJCOSX level of theory using UKS wave-functions.[74]

We found that the geometry of the T_1 state is not aromatic and reproduces the vinylic structure hypothesized to be a product of the degradation mechanism. This is in agreement with Baird's rule.[75] This said, one can describe the molecular orbital diagram for the involved electronic transition as in Figure 14.
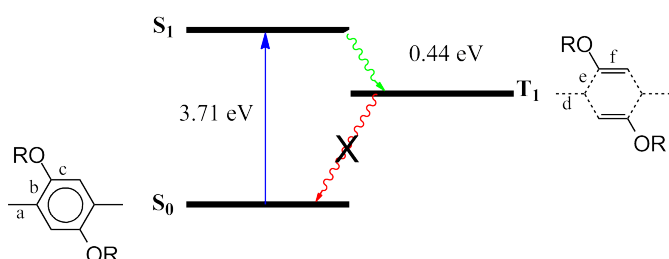

Figure 14. Molecular orbital diagram for the first photo-excitation of the comonomer depicted in the inset.

One should observe that the comonomer is aromatic in the S_0 state and the first photo-excitation takes place with a calculated photon-energy of $\sim$ 3.7 eV ($\sim$ 335 nm). Once in the S_1 state, the excited electron can relax thermally and by successive intersystem crossing (ISC) reach the T_1 state, where it has an anti-aromatic structure. This is believed to be the origin of the destabilization of the comonomer-fullerene bond. The bond lengths a, b and c are 1.51, 1.40 and 1.40 Å, respectively, for the molecules in the S_0 state, and 1.50, 1.50 and 1.37 Å, for d, e and f, respectively, for the molecules in the T_1 state. These results indicate that the absorption of light by the comonomer leads, in this case, to an anti-bonding-like structure where both fullerene and comonomers are not linked any longer. Considering the error that may have been induced by TD-DFT calculations in the determination of the S_1 state, one should estimate that wavelengths between 330 and 380 nm are enough to break this bond.

3   Conclusions

This work has shown that PFBMBs are relatively unstable and that this is due to a weak methylene-C_{60} bond. Their behaviour is in contrast to other PFs, such as those formed via the SACAP route which have demonstrated exceptional stabilities. Interestingly, the behaviour seen for PFBMBs in this work is also in contrast to analogous weakly linked methylene-C_{60} polymers incorporating PCBM into the main-chain, which have been shown to stabilise photovoltaic devices. This might simply be due to an equilibrium process being maintained, or due to the PCBM carrying a larger number of atoms and thus being able to act as a vibrator to liberate thermal energy away from the weak methylene-fullerene bond.

However, to sum, when employing PFs, the nature of the link between the C_{60} and the comonomer should be chosen with care as it impacts greatly on the stability of the polymers. While this may render PFBMBs in appropriate for photovoltaics, it might mean that they are more appropriate for other applications, for example in medicine, where the *in-situ* liberation of C_{60} molecules is required.

4   Acknowledgements

5   References

1. a) T. Wang, A. J. Pearson and D. G. Lidzey, *J. Mater. Chem. C*, **2013**, *1*, 7266; b) T. Xiao, H. Xu, G. Grancini, J. Mai, A. Petrozza, U.-S. Jeng, Y. Wang, X. Xin, Y. Lu, N. S. Choon, H. Xiao, B. S. Ong, X. Lu, N. Zhao, *Scientific Reports*, **2014**, *4*, 5211.
2. X. Yang, J. Loos, S. C. Veenstra, W. J. H. Verhees, M. M. Wienk, J. M. Kroon, M. A. J. Michels and R. A. J. Janssen, *Nano letters*, **2005**, *5*, 579.
3. (a) B. Xue, B. Vaughan, C.-H. Poh, K. B. Burke, L. Thomsen, A. Stapleton, X. Zhou, G. W. Bryant, W. Belcher and P. C. Dastor, *J. Phys. Chem. C*, **2010**, *114*, 15797; (b) M. Campoy-Quiles, T. Ferenczi, T. Agostinelli, P. G. Etchegoin, Y. Kim, T. D. Anthopoulos, P. N. Stavrinou, D. D. C. Bradley and J. Nelson, *Nat Mater* **2008**, *7*, 158.
4. J. Zhao, A. Swinnen, G. Van Assche, J. Manca, D. Vanderzande and B. Van Mele, *J. Phys. Chem. B* **2009,** *113*, 1587.
5. (a) E. Verploegen, R. Mondal, C. J. Bettinger, S. Sok, M. F. Toney and Z. Bao, *Adv. Funct. Mater.*, **2010**, *20*, 3519; (b) Y. Kim, S. A. Choulis, J. Nelson, D. D. C. Bradley, S. Cook, J. R. Durrant, *Appl. Phys. Lett.* **2005**, *86*, 063502; (c) K. Vegso, P. Siffalovic, M. Jergel, P. Nadazdy, V. Nadazdy and E. Majkova, *ACS Applied Materials & Interfaces* **2017**, *9*, 8241.
6. (a) J. K. Lee, W. L. Ma, C. J. Brabec, J. Yuen, J. S. Moon, J. Y. Kim, K. Lee, G. C. Bazan and A. J. Heeger, *J. Am. Chem. Soc.,* **2008**, *130*, 3619; (b) A. J. Heeger, *Adv. Mater.,* **2014**, *26*, 10.
7. J. Ahmad, K. Bazaka, L. J. Anderson, R. D. White and M. V. Jacob, *Renewable and Sustainable Energy Reviews*, **2013**, *27*, 104.
8. M. Jørgensen, K. Norrman and F. C. Krebs, *Solar Energy Materials and Solar Cells*, **2008**, *92*, 686.
9. '*OPV materials are robust and stable over decades*, OPVIUS GmbH', **2018**, at http://www.opvius.com/en/stability.html (accessed April 2019).
10. H. Santos Silva, A. Tournebize, D. Bégué, H. Peisert, T. Chassé, J.-L. Gardette, S. Therias, A. Rivaton and R. C. Hiorns, *RSC Advances*, **2014**, *4*, 54919.
11. Y. W. Soon, H. Cho, J. Low, H. Bronstein, I. McCulloch and J. R. Durrant, *Chem. Commun.*, **2013**, *49*, 1291.
12. J. A. Moore, S. Ali and B. C. Berry, *Solar Energy Materials and Solar Cells*, **2013**, *118*, 96.
13. S. A. Dowland, M. Salvador, J. Darío Perea, N. Gasparini, S. Langner, S. Rajoelson, H. H. Ramanitra, B. D. Lindner, A. Osvet, C. J. Brabec, R. C. Hiorns and H. -J. Egelhaaf, *ACS Applied Materials & Interfaces*, **2017**, *9*, 10971. DOI: 10.1021/acsami.7b00401
14. N. Gasparini, A. Wadsworth, M. Moser, D. Baran, I. McCulloch and C. J. Brabec, *Adv. Energy Mater*. **2018**, 1703298.
15. L. Meng, Y. Zhang, X. Wan, C. Li, X. Zhang, Y. Wang, X. Ke, Z. Xiao, L. Ding, R. Xia, H.-L. Yip, Y. Cao and Y. Chen, *Science*, **2018**, 361, 1094.
16. L. Derue, O. Dautel, A. Tournebize, M. Drees, H. Pan, S. Berthumeyrie, B. Pavageau, E. Cloutet, S. Chambon, L. Hirsch, A. Rivaton, P. Hudhomme, A. Facchetti, G. Wantz, *Adv. Mater.*, **2014**, *26*, 5831.
17. H. Hoppe and N. S. Sariciftci, *J. Mater. Chem.*, **2006**, *16*, 45.
18. R. A. J. Janssen, J. C. Hummelen and N. S. Sariciftci, *MRS bulletin*, **2005**, *30*, 33.
19. G. E. Morse, A. Tournebize, A. Rivaton, T. Chassé, C. Taviot-Guého, N. Blouin, O. R. Lozman and S. Tierney, *Phys. Chem. Chem. Phys.* **2015**, *17*, 11884.
20. (a) C. Lindqvist, J. Bergqvist, C.-C. Feng, S. Gustafsson, O. Bäcke, N. D. Treat, C. Bounioux, P. Henriksson, R. Kroon, E. Wang, A. Sanz-Velasco, P. M. Kristiansen, N. Stingelin, E. Olsson, O. Inganäš, M. R. Andersson and C. Müller, *Adv. Energy Mater.*, **2014**, *4*, 1301437; (b) N. D. Treat, J. A. Nekuda Malik, O. Reid, L. Yu, C. G. Shuttle, G. Rumbles, C. J. Hawker, M. L. Chabinyc, P. Smith and N. Stingelin, *Nature Materials*, **2013**, *12*, 628.
21. T. Heumueller, W. R. Mateker, A. Distler, U. F. Fritze, R. Cheacharoen, W. H. Nguyen, M. Biele, M. Salvador, M. von Delius, H.-J. Egelhaaf, M. D. McGehee and C. J. Brabec, *Energy Environ. Sci.* **2015**, *9*, 247.
22. H. H. Ramanitra, S. A. Dowland, B. A. Bregadiolli, M. Salvador, H. Santos Silva, D. Bégué, C. F. O. Graeff, H. Peisert, T. Chassé, S. Rajoelson, A. Osvet, C. J. Brabec, H.-J. Egelhaaf, G. E. Morse, A. Distler and R. C. Hiorns, *J. Mater. Chem. C* **2016**, *4*, 8121.
23. P. D. Topham, A. J. Parnell, R. C. Hiorns, *J. Polym. Sci. B Polym. Phys.* **2011**, *49*, 1131.
24. M. Raïssi, H. Erothu, E. Ibarboure, H. Bejbouji, H. Cramail, E. Cloutet, L. Vignau and R. C. Hiorns, *J.*

Mater. Chem. A, **2017**, *5*, 7533.

25. (a) Y.-G. Ko, S. G. Hahm, K. Murata, Y. Y. Kim, B. J. Ree, S. Song, T. Michinobu and M. Ree, *Macromolecules*, **2014**, *47*, 8154; (b) H. Ito, Y. Ishida and K. Saigo, *Tetrahedron Letters* **2006**, *47*, 3095.
26. (a) F. Giacalone and N. Martín, *Chem. Rev.* **2006**, *106*, 5136; (b) K. E. Geckeler and S. Samal, *Polym. Int.,* **1999**, *48*, 743.
27. D. Loy and R. Assink, *J. Am. Chem. Soc* **1992**, *114*, 3977.
28. A. Gogel, P. Belik, M. Walter, A. Kraus, E. Harth, M. Wagner, J. Spickermann, K. Müllen, *Tetrahedron,* **1996**, *52*, 5007.
29. S. Samal, B.-J. Choi and K. E. Geckeler, *Chem. Commun.* **2000**, 1373.
30. M. Stephen, H. H. Ramanitra, H. Santos Silva, S. A. Dowland, D. Bégué, K. Genevius, K. Arlauskas, G. Juska, G. E. Morse, A. Distler and R. C. Hiorns, *Chem. Commun.* **2016**, *52*, 6107.
31. (a) H. H. Ramanitra, H. Santos Silva, B. A. Bregadiolli, A. Khoukh, C. M. S. Combe, S. A. Dowland, D. Bégué, C. F. O. Graeff, C. Dagron-Lartigau, A. Distler, G. E. Morse and R. C. Hiorns, *Macromolecules* **2016**, *49*, 1681. b) M. Stephen, S. A. Dowland, A. Gregori, H. H. Ramanitra, H. Santos Silva, C. M. S. Combe, D. Bégué, C. Dagron-Lartigau, G. E. Morse, K. Genevičius, K. Arlauskas, G. Juška, A. Distler and R. C. Hiorns, *Polym. Int.* **2017**, *66*, 388.
32. B. A. Bregadiolli, H. H. Ramanitra, R. M. Ferreira, L. Corcoles, M. S. Gomes, L. Kang, C. M. S. Combe, H. Santos Silva, F. C. Lavada, D. Bégué, C. Dagron-Lartigau, M. L. M. Rocco, C. K. Luscombe, C. Olivati, C. F. O. Graeff and R. C. Hiorns, *Polym. Int.,* **2017**, *66*, 1364.
33. (a) R. C. Hiorns, E. Cloutet, E. Ibarboure, L. Vignau, N. Lemaître, S. Guillerez, C. Absalon and H. Cramail, *Macromolecules* **2009**, *42*, 3549. (b) R. C. Hiorns, E. Cloutet, E. Ibarboure, A. Khoukh, H. Bejbouji, L. Vignau and H. Cramail, *Macromolecules* **2010**, *43*, 6033.
34. H. Santos Silva, H. H. Ramanitra, B. A. Bregadiolli, D. Bégué, C. F. O. Graeff, C. Dagron-Lartigau, H. Peisert, T. Chassé and R. C. Hiorns, *J. Polym. Sci. Part A: Polym. Chem.* **2017**, *55*, 1345.
35. A. Tournebize, P.-O. Bussière, P. Wong-Wah-Chung, S. Thérias, A. Rivaton, J.-L. Gardette, S. Beaupré and M. Leclerc, *Adv. Energy Mater.*, **2013**, *3*, 478.
36. R. Taylor, J. P. Parsons, A. G Avent, S. P. Rannard, T J. Dennis, J. P. Hare, H. W. Kroto and D. R. M. Walton, *Nature*, **1991**, 351, 277.
37. S. Chambon, A. Rivaton, J.-L. Gardette and M. Firon. *Sol. Energy Mater. & Solar Cells*, **2007**, 91, 394.
38. S. Fukuzumi, H. Mori, T. Suenobu, H. Imahori, X. Gao and K. M. Kadish, *J. Phys. Chem. A*, **2000**, *104*, 10688.
39. S. Fukuzumi, T. Suenobu, X. Gao and K. M Kadish, *J. Phys. Chem. A*, **2000**, *104*, 2908.
40. K. M. Kadish, X. Gao, E. Van Caemelbecke, T. Suenobu and S. Fukuzumi, *J. Am. Chem. Soc.*, **2000**, *122*, 563.
41. K. M. Kadish, X. Gao, E. Van Caemelbecke, T. Hirasaka, T. Suenobu and S. Fukuzumi, *J. Phys. Chem. A*, **1998**, *102*, 3898.
42. H. Wang, Y, He, Y. Li and H. Su, *J. Phys. Chem. A*. **2012**, *116*, 255.
43. Y. Tan and D. E Resasco, *J. Phys. Chem. B*, **2005**, *109*, 14454.
44. H. Santos Silva, J. Cresson, A. Rivaton, D. Bégué and R. C. Hiorns, *Org. Electron.* **2015**, *26*, 395.
45. (a) S. G. Penn, D. A. Costa, A. L. Balch and C. B. Lebrilla, *Int J Mass Spectrom Ion Processes* **1997**, **169**–**170**, 371; (b) I. E. Brumboiu, L. Ericsson, R. Hansson, E. Moons, O. Eriksson and B. Brena, *J. Chem. Phys.*, **2015**, *142*, 054306.
46. F. Piersimoni, G. Degutis, S. Bertho, K. Vandewal, D. Spoltore, T. Vangerven, J. Drijkoningen, M. K. Van Bael, A. Hardy, J. D'Haen, *et al*. *J. Polym. Sci. Pt B: Polym. Phys.*, **2013**, *51*, 1209.
47. A. Distler, T. Sauermann, H.-J. Egelhaaf, S. Rodman, D. Waller, K.-S. Cheon, M. Lee and D. M. Guldi, *Adv. Energy Mater.*, **2014**, *4*, 1300693.
48. H. C. Wong, Z. Li, C. H. Tan, H. Zhong, Z. Huang, H. Bronstein, I. McCulloch, J. T. Cabral and J. R. Durrant, *ACS Nano*, **2014**, *8*, 1297.
49. A. Kumar, F. Singh, Govind, S. M. Shivaprasad, D. K. Avasthi, J. C. Pivin, *et al*. *Appl. Surf. Sci.*, 2008, *254*, 7280.
50. (a) A. M. Rao, P. Zhou, K. A. Wang, G. T. Hager, J. M. Holden, Y. Wang, W. T. Lee, X.-X. Bi, P. C. Eklund, D. S. Cornett, *Science* **1993**, *259*, 955; (b) P. Eklund, A. M. Rao, P. Zhou, Y. Wang and J. M. Holden, *Thin Solid Films* **1995**, *257*, 185.
51. S. G. Penn, D. A. Costa, A. L. Balch and C. B. Lebrilla, *Int. J. Mass Spectrom. Ion Processes*, **1997**,

169/170, 371.

52. W. Krätschmer, L. D. Lamb, K. Fostiropoulos and D. R. Huffman, *Nature*, **1990**, *347*, 354.

53. H. Yamawaki, M. Yoshida, Y. Kakudate, S. Usuba, H. Yokoi, S. Fujiwara, K. Aoki, R. Ruoff, R. Malhotra and D Lorents, *J. Phys. Chem.*, **1993**, *97*, 11161.

54. A. Rivaton, S. Chambon, M. Manceau, J.-L. Gardette, N. Lemaître and S. Guillerez, *Polymer Degradation and Stability*, **2010**, *95*, 278.

55. N. Sai, K. Leung, J. Zádor and G. Henkelman, *PhysChemChemPhys.*, **2014**, *16*, 8092.

56. H. Hintz, C. Sessler, H. Peisert, H.-J. Egelhaaf and T. Chassé, *Chem. Mater.*, **2012**, *24*, 2739.

57. M. Manceau, A. Rivaton, J.-L. Gardette, S. Guillerez and N. Lemaître, *Sol. Energy Mater. & Solar Cells*, **2011**, *95*, 1315.

58. H. Hintz, H.-J. Egelhaaf, L. Lüer, J. Hauch, H. Peisert and T. Chassé, *Chem. Mater.*, **2010**, *23*, 145.

59. H. Hintz, H. Peisert, H.-J. Egelhaaf and T. Chassé, *J. Phys. Chem. C*, **2011**, *115*, 13373.

60. P. Song, Y. Zhu, L. Tong and Z. Fang, *Nanotechnology*, **2008**, *19*, 225707.

61. M. D. Tzirakis and M. Orfanopoulos, *Chem. Rev.*, **2013**, *113*, 5262.

62. E. B. Zeynalov and J. F. Friedrich, *Materials Testing*, **2007**, *49*, 265.

63. D. Pantazis, S. Pispas and N. Hadjichristidis, *J. Polym. Sci. Pt A: Polym. Chem.*, **2001**, *39*, 2494.

64. C. Mathis, S. Nunige, F. Audouin and R. Nuffer, *Synthetic Metals*, **2001**, *121*, 1153.

65. C. Mathis, B. Schmaltz and M. Brinkmann, *Comptes Rendus Chimie*, **2006**, *9*, 1075.

66. O. F. Pozdnyakov, B. P. Redkov, G. K. Lebedeva, L. S. Litvinova, V. N. Ivanova, A. O. Pozdnyakov and V. V. Kudryavtsev, *Technical Physics Letters*, **2002**, *28*, 188.

67. O. F. Pozdnyakov, A. O. Pozdnyakov, B. Schmaltz and C. Mathis, *Polymer*, **2006**, *47*, 1028.

68. B. M. Ginzburg, A. O. Pozdnyakov, V. N. Zgonnik, O. F. Podzdnyakov, B. P. Redkov, E. Y. Melenevskaya and L. V. Vinogradova, *Technical Physics Letters*, **1996**, *22*, 166.

69. A. O. Pozdnyakov, O. F. Pozdnyakov, B. P. Redkov, V. N. Zgonnik, L. V. Vinogradova, E. Y. Melenevskaya and B. M. Ginzburg, *Technical Physics Letters*, **1996**, *22*, 759.

70. F. Audouin, R. Nuffer and C. Mathis, *J. Polym. Sci. Pt A: Polym. Chem.*, **2004**, *42*, 4820.

71. T.-H. Zhang, P. Lu, F. Wang and G.-Wu Wang, *Organic & Biomolecular Chemistry*, **2003**, *1*, 4403.

72. a) J. D. Nikolić, S. Wouters, J. Romanova, A. Shimizu, B. Champagne, T. Junkers, D. Vanderzande, D. Van Neck, M. Waroquier, V. Van Speybroeck and S. Catak, *Chem. Eur. J.,* **2015**, *21*, 19176; b) T. Schwalm and M. Rehahn, *Macromolecules*, **2007**, *40*, 3921; c) L. Hermosilla, S. Catak, V. Van Speybroeck, M. Joke Vandenbergh, F. Motmans, P. Adriaensens, L. Lutsen, T. Cleij and D. Vanderzande, *Macromolecules*, **2010**, *43*, 7424.

73. R. C. Hiorns, E. Cloutet, E. Ibarboure, A. Khoukh, H. Bejbouji, L. Vignau and H. Cramail, *Macromolecules* **2010**, *43*, 6033.

74. F. Neese, F. Wennmohs, A. Hansen, U. Becker, Efficient, Approximate and Parallel Hartree–Fock and Hybrid DFT Calculations. A 'Chain-of-Spheres' Algorithm for the Hartree–Fock Exchange', *Chem. Phys.* **2009**, 356, 98.

75. N. C. Baird, *J. Am. Chem. Soc.*, **1972**, *94*, 4941.